Polymer 254 (2022) 125070

Contents lists available at ScienceDirect

Polymer

journal homepage: www.elsevier.com/locate/polymer

Carbazole-conjugated microporous polymers from Suzuki–Miyaura coupling for supercapacitors

Ahmed F. Saber [a,b], Santosh U. Sharma [c], Jyh-Tsung Lee [c], Ahmed F.M. EL-Mahdy [a,*], Shiao-Wei Kuo [a,d]

[a] Department of Materials and Optoelectronic Science, National Sun Yat-Sen University, Kaohsiung, 80424, Taiwan
[b] Department of Chemistry, Faculty of Science, Assiut University, Assiut, 71516, Egypt
[c] Department of Chemistry, National Sun Yat-Sen University, Kaohsiung, 80424, Taiwan
[d] Department of Medicinal and Applied Chemistry, Kaohsiung Medical University, Kaohsiung, 807, Taiwan

ARTICLE INFO

Keywords:
Conjugated microporous polymers (CMPs)
Carbazole-based CMPs
Suzuki-miyaura coupling
Energy storage

ABSTRACT

Conjugated microporous polymers (CMPs) were intensively exploited for many applications including optoelectronics, CO_2 adsorption, and catalysis. Nevertheless, CMPs based electrochemical supercapacitors as energy storing systems were largely unreconnoitered yet. This may be attributed mainly to some drawbacks relating to low structural/electrochemical stabilization, and somewhat poor specific capacitance, in addition to depressed energy density observed for most of the discovered CMPs. In this work, a set of novel carbazole-based CMPs with redox activity, Cz-Cz CMP, Cz-TPA CMP and Cz-TP CMP, have been successfully prepared and examined as dynamic electrodes for supercapacitors. The as-synthesized Cz-Cz and Cz-TPA CMPs possessed the highest and very close values of specific surface areas of 623 and 618 $m^2\ g^{-1}$, respectively, with the corresponding pore sizes centered at of 0.49 and 0.40 nm, respectively. The electrochemical study of all CMPs has been measured by both cyclic voltammetry (CV), and galvanostatic charge/discharge (GCD). The obtained CV curves resembled rectangle shapes, suggesting a typical electric double-layer manner over the potential range and the scan rates. The Cz-TPA CMP were the best candidate with an electrochemical capacity of 271.82 F g^{-1} at 0.5 A g^{-1} current density, and rapid rate of charge/discharge cycle. In addition, it owned the excellence in cycling stability that was displayed to retain 99.87% of the capacitance after 2000 cycling times at 10 A g^{-1}. From all analysis data, one can conclude that, our polymers were among the best stable electrode materials.

1. Introduction

Currently, environmental issues linked to the burning of large amounts of petroleum fuels, such as excessive CO_2 emissions, and the hazardous particulates released from automotive exhausts, have resulted in another environmental problem: climate change [1]. Consequently, scientists focused on solving this situation by finding novel and efficient alternates of renewable energy storage [2,3]. One of the most convenient solutions for energy shortage was the electrochemical energy storage [4]. Various devices based on electrochemistry principle have been emerged, ranging from rechargeable batteries, to classical capacitors and supercapacitors (SCs) with good features including, safety, reasonable capacity intensity, rapid charge/discharge kinetics, and high cycle stability [5,6]. SCs were the most advanced and promising type for this purpose with other key advantages, like cheapness, outstanding lifespan, and excellent rate efficiency [7–10]. There are two mechanisms for storing energy in SCs. The first one follows the non-faradaic procedures, in which the electrostatic ionic charges were aggregated at the interface between electrolyte and electrode. The second mechanism is the faradaic processes, that takes place at the solid surface via the reversible redox reaction [11,12]. Therefore, the electrode material is considered from the master parameters affecting the efficacy of SCs [13]. Inorganic metal oxides, doped carbon, conjugated polymers, and organic polymeric molecules such as covalent organic frameworks (COFs), covalent triazine frameworks (CTFs), and hyper-crosslinked polymers have been applied as electrodes for SCs [14–26]. Unfortunately, inorganic materials have a number of disadvantages, including resources scarcity and environmental contaminations.

In comparison, conjugated polymers (CPs) were deemed the

* Corresponding author.
E-mail addresses: ahmedelmahdy@mail.nsysu.edu.tw (A.F.M. EL-Mahdy), kuosw@faculty.nsysu.edu.tw (S.-W. Kuo).

https://doi.org/10.1016/j.polymer.2022.125070
Received 5 April 2022; Received in revised form 6 June 2022; Accepted 12 June 2022
Available online 17 June 2022

cheapest solution for using as electrodes in SCs. For instance, polyaniline possessed specific capacitance as 1221 F g^{-1} [27], which is much higher than that of activated carbon electrode (<200 F g^{-1}) [28], and ruthenium oxide (1170 F g^{-1}) [29]. However, conventional CPs like polyaniline possessed no porosity and not robust owing to their degradation after few cycles [30]. On the other hand, organo-electrodes have aroused more interests due to their excellent features such as good electrochemical efficiency, minimum energy consuming, and ecological friendly [31–33]. Conjugated microporous materials (CMPs), a form of organic polymers, were among the most commonly used in SCs due to its unique properties such as structural tunability, pore structures variety, physicochemical stability, and delocalized conjugation [34,35]. Besides their various applications in gas uptake and separation, dye adsorption, organic photovoltaic, photocatalysis, energy and environmental fields [36–43], they are also used as superior electrodes in SCs [44–50]. Introducing of nitrogen heteroatom has the ability to improve wettability and conductivity of CMP-electrode, in addition to endowing pseudo-capacitance to the electrode which further enhances the electrochemical efficiency [51,52].

Herein, three novel CMPs have been synthesized by adopting carbazole-based crosslinker (Cz-3BO) to react with various di- and tribromo monomers; namely: Cz-3Br, TPA-3Br, and TP-2Br. The produced porous polymers displayed not only high specific surface areas and thermal stabilities, but also represented excellent electrochemical behavior reaching to 271.82 F g^{-1} as the best obtained value.

2. Results and discussions

The participating monomers 3,6-dibromo-9-(4-bromophenyl)-9H-carbazole (Cz-3Br), tris(4-bromophenyl)amine (TPA-3Br) and 5,7-dibromothieno[3,4-*b*]pyrazine (TP-2Br) have been prepared according to literature procedures (Schemes S1–S3) [53–55]. Whereas the prime utilized monomer 3,6-bis(4,4,5,5-tetramethyl-1,3,2-dioxaborolan-2-yl)-9-(4-(4,4,5,5-tetramethyl-1,3,2- dioxaborolan-2-yl)phenyl)-9H-carbazole (Cz-3BO) has been synthesized through Suzuki-Miyaura chemical reaction as drawn in Scheme S4. The condensation reaction between -9HCz-3Br with bis(pinacolato)diboron was applied using [1,1′-bis(diphenylphosphino)ferrocene]dichloropalladium(II) catalyst at a definite temperature 110 °C in dioxane solvent containing potassium acetate, to afford the desired Cz-3BO in a very good yield. The chemical structure of this major building block was affirmed through many analyses, such as the Fourier transform infrared (FTIR) and nuclear magnetic resonance (NMR) techniques. FTIR spectrum of Cz-3BO displayed the complete disappearance of absorption band at 630 cm^{-1} for C–Br bond of the corresponding bromide derivative Cz-3Br (Fig. S1), and the generation instead of other spectral bands at 3045, 2981, 2928 and 1350 cm^{-1} characteristic of C–H aromatic, C–H aliphatic

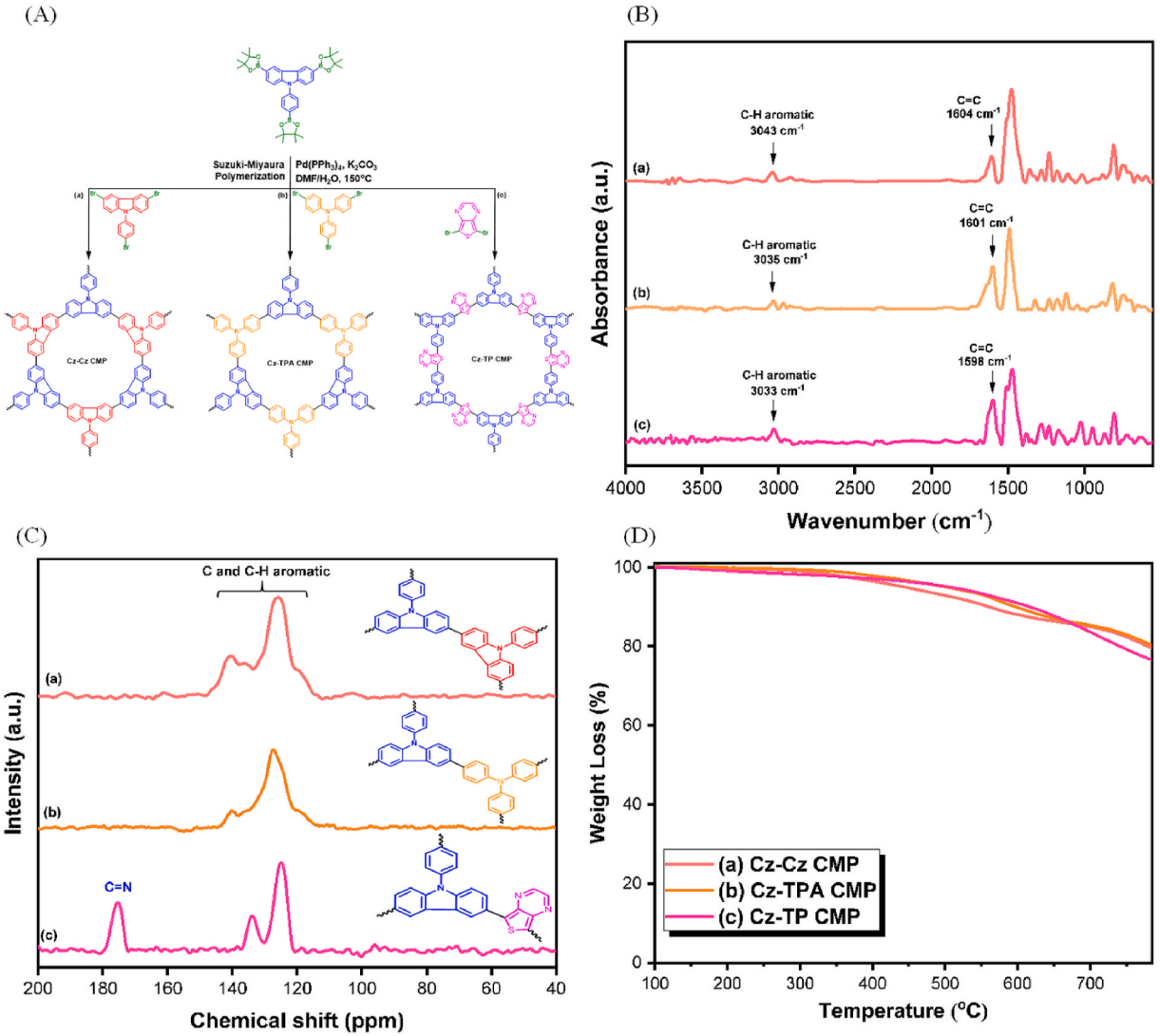

Fig. 1. (A) Chemical synthesis of (a) Cz-Cz, (b) Cz-TPA, and (c) Cz-TP CMPs. (B) FTIR spectra of the as-prepared (a) Cz-Cz, (b) Cz-TPA, and (c) Cz-TP CMPs. (C) Solid state ^{13}C NMR spectra of (a) Cz-Cz, (b) Cz-TPA, and (c) Cz-TP CMPs. (D) TGA curves of the studied polymers (a) Cz-Cz, (b) Cz-TPA, and (c) Cz-TP CMPs.

and B–O stretching vibrations, respectively (Fig. S2). In addition, the ^{1}H NMR spectrum of Cz-3BO indicated the presence of two singlet signals corresponding to phenyl rings at 8.06 and 8.15 ppm, as well as an additional singlet signal corresponding to methyl protons at 1.4 ppm (Fig. S3). Subsequently, the ^{13}C NMR spectrum of Cz-3BO represented some signals in the range 128.41–140.20 ppm which were identified to carbon atoms of phenyl rings, besides two intense peaks assigned to pinacolato carbon nuclei at 83.52 and 24.31 ppm (Fig. S4). The electrochemical active CMPs holding carbazole building block have been constructed via Pd catalysis Suzuki coupling reaction of the master compound (Cz-3BO) with the above stated three synthesized monomers, Cz-3Br, TPA-3Br, and TP-2Br, respectively, in a co-solvent of DMF and H_2O (8:1, v/v) at a temperature 145 °C, in the presence of K_2CO_3 in the reaction medium, as depicted in (Fig. 1A and Schemes S5-S7). Chemical characterization of the yielded conjugated polymers was also accomplished by the utilization of conventional FTIR and solid state ^{13}C NMR techniques. The composition of the generated polymeric frameworks was initially examined using FTIR spectra, which revealed that certain absorption bands centered at 2981, 2928, and 1350 cm^{-1}, indicative of C–H aliphatic and B–O typical stretching vibrations for Cz-3BO major monomer were perfectly passed. Furthermore, the sharp C–Br absorption bands at 630, 666, and 626 cm^{-1}, which correspond to the implicated monomers Cz-3Br, TPA-3Br, and TP-2Br, respectively, vanished (Fig. 1B and Figs. S5-S7). Solid state ^{13}C NMR was also used to determine the typical polymerization between monomeric components leading to polymeric networks. There were no signals for pinacolato carbon nuclei, but there were broad peaks for aromatic carbons in the ranges of 114–146 ppm, 115–149 ppm, and 119–136 ppm, respectively, corresponding to Cz-Cz CMP, Cz-TPA CMP, and Cz-TP CMP. In addition, a sharp signal was observed at 175 ppm which assigned to C═N carbon of Cz-TP CMP (Fig. 1C). The most prevalent property of these CMPs has been noticed in their stiffness and high degree of crosslinking, which resulted in a significant reduction in solubility and increasing of thermal stability. For the application of our synthesized polymeric frameworks, their thermal stabilities were investigated using thermogravimetric analysis technique (TGA). This measurement was evaluated under a nitrogen stream at a temperature ranging from ambient temperature to 800 °C. As described in (Fig. 1D), all of the three CMPs under study possessed considerable thermal stabilities, in which Cz-TP CMP represented the top value with a negligible weight loss of nearly 10% (T_{d10}) up to 616 °C as a consequence of organic groups decomposition. On the other bank, Cz-Cz CMP had the floor thermal stability value which was located at 560 °C under the same conditions, whilst, Cz-TPA CMP lies on an intermediate distance from them with maintaining its stability till 597 °C. To complete this study, we also monitored the produced char yield, Cz-Cz and Cz-TPA CMPs have nearly the same char yield with observed amounts of 79 and 80%, respectively, whereas the Cz-TP polymer owned a little small amount than them up to 76% (Table S1).

Nitrogen gas sorption assays at 77 K were used to assess the manifest surface areas and porosity properties of the as-synthesized polymers (Table 1). The microporous structures for the obtained CMPs were depicted in [Fig. 2(a-c)], which displayed the type I isothermal curves with a decline N_2 adsorption at low relative pressure (P/P_0). A hysteresis loop was appeared in the figures which considered as an indication of a hierarchical network structures with a high microporosity degree. Furthermore, when the relative pressure reached 0.8, nitrogen adsorption increased significantly, implying the presence of some macropores in addition to the main micropores. This could be attributed to the interparticulate gaps caused by the loose packing of tiny particles, as shown in the SEM images (Fig. 3(a–c)). The produced CMPs exhibited calculated BET surface areas with excellent outputs which ranged from the minimum value at 412 $m^2 g^{-1}$ for Cz-TP CMP, and 618 $m^2 g^{-1}$ for Cz-TPA CMP, to the highly porous Cz-Cz CMP with a maximum value estimated at 623 $m^2 g^{-1}$. The nonlocal density functional theory was applied to estimate the pore volumes of the polymers, which were calculated to be 0.49 $cm^3 g^{-1}$ for Cz-Cz CMP, 0.40 $cm^3 g^{-1}$ for Cz-TPA CMP and the lowest value for Cz-TP CMP as 0.38 $cm^3 g^{-1}$. From the illustration, we can see that both Cz-Cz and Cz-TPA CMPs show uniform pore size and the pore diameter is mainly around 1.4 nm. Finally, the pore size distribution of the measured samples represents their pore diameters as 1.40 nm, 1.29 nm, and 1.03 nm corresponding to Cz-Cz, Cz-TPA, and Cz-TP CMPs, respectively, [Fig. 2(d-f)]. As we showed before, Cz-Cz and Cz-TP have the top and floor values of specific surface areas, respectively, (Table 1), this behavior could be referred to the difference degree of cross-linking of the polymers. The reactive connectivity of the initial monomers varies, ranging from three-substituted active locations like Cz-3Br and TPA-3Br to two-substituted active positions like TP-2Br. Besides that, Cz-Cz CMP displayed the highest surface area (623 $m^2 g^{-1}$) which is very close to that of Cz-TPA CMP (618 $m^2 g^{-1}$) because both of them nearly have the same shorter monomer length. On the other side, the longer monomer length of TP-2Br reflected in a minimum surface area of the corresponding Cz-TP CMP (412 $m^2 g^{-1}$).

Table 1
BET parameters of the as-prepared CMPs.

CMPs	SBET ($m^2 g^{-1}$)	Pore size (nm)	Pore volume ($cm^3 g^{-1}$)
Cz-Cz CMP	623	1.40	0.49
Cz-TPA CMP	618	1.29	0.40
Cz-TP CMP	412	1.03	0.38

The morphological character for the produced CMPs was examined using a scanning electron microscope (SEM) in conjunction with a transmission electron microscope (TEM). The irregular stacking morphologies of polymeric surfaces was proved and represented by SEM, in which they were homogeneous and consisting of small spherical particles with loosely packing. In other words, aggregated tiny particles with nano-scaled diameters were observed. As previously demonstrated in BET investigations, this shape may supply some outside macropores originating from interstitial gaps [Fig. 3(a-c)]. In addition, TEM displayed and confirm the microporous structures for the CMPs which resulted from the highly cross-linked frameworks. Spherical shaped nanoparticles have been recognized with an internal diameter in the range of 100–500 nm. The HR-TEM investigation of the resultant polymeric materials exhibited both the amorphous and porous properties [Fig. 3(d-f)].

3. Electrochemical performance

The electrochemical behavior of the carbazole-bearing CMPs has been studied by the utilization of both cyclic voltammetry (CV), galvanostatic charge/discharge (GCD) in a system containing three electrodes immersed in aqueous H_2SO_4 (1 M) as electrolyte. The potential used for examination of the CV performance was in the range between 0.1 and 0.6 V at several sweep rates from the value of 5 mV/s to 200 mV/s [Fig. 4 (a-c)]. The obtained CV curves of the tested samples resembled rectangle shapes, suggesting a typical electric double-layer manner over the potential range as well as the scan rates. The calculated specific capacitance was resulted from the capacitance *vs.* scan rates plot, with the maximum capacitance value at 271.82 F g^{-1} for Cz-TPA CMP, whereas, the Cz-Cz, and Cz-TP CMPs displayed the lower values of capacitance which located at 43.70 F g^{-1} (at 0.5 A) and 67.38 F g^{-1}(at 1 A), respectively, all measured at 5 mV/s scan rate [Fig. 5(a)]. As represented in BET analysis, Cz-Cz CMP has the highest surface area (623 $m^2 g^{-1}$), the largest pore size (1.40 nm) than the corresponding values of Cz-TPA and Cz-TP, that facilitate the penetration of ions to the electrode surface. As a consequence, a quick electrolytic ions transfer was happened at the electrode/electrolyte interface [56,57], resulting in a notable electric double layer capacitance (EDLC) efficiency for Cz-Cz CMP. Interestingly, Cz-TP CMP owned the lowest surface area and pore size as well, but demonstrated a higher capacitance value compared to Cz-Cz CMP. This attitude can be explained in terms of increasing the nitrogen content in Cz-TP CMP compared to Cz-Cz CMP, which is directly proportional to the capacitance performance [24]. Although Cz-Cz, and Cz-TPA CMPs

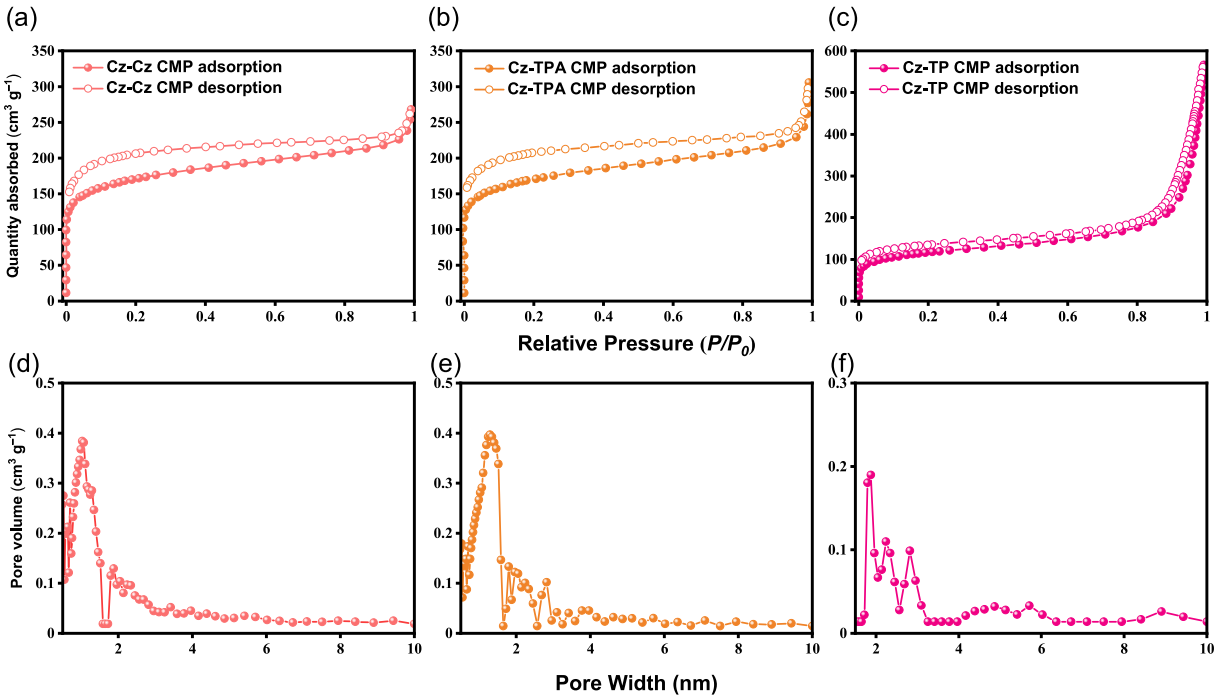

Fig. 2. N_2 sorption isotherms of (a) Cz-Cz, (b) Cz-TPA, and (c) Cz-TP CMPs; The corresponding pore size distribution curves of (d) Cz-Cz, (e) Cz-TPA, and (f) Cz-TP CMPs.

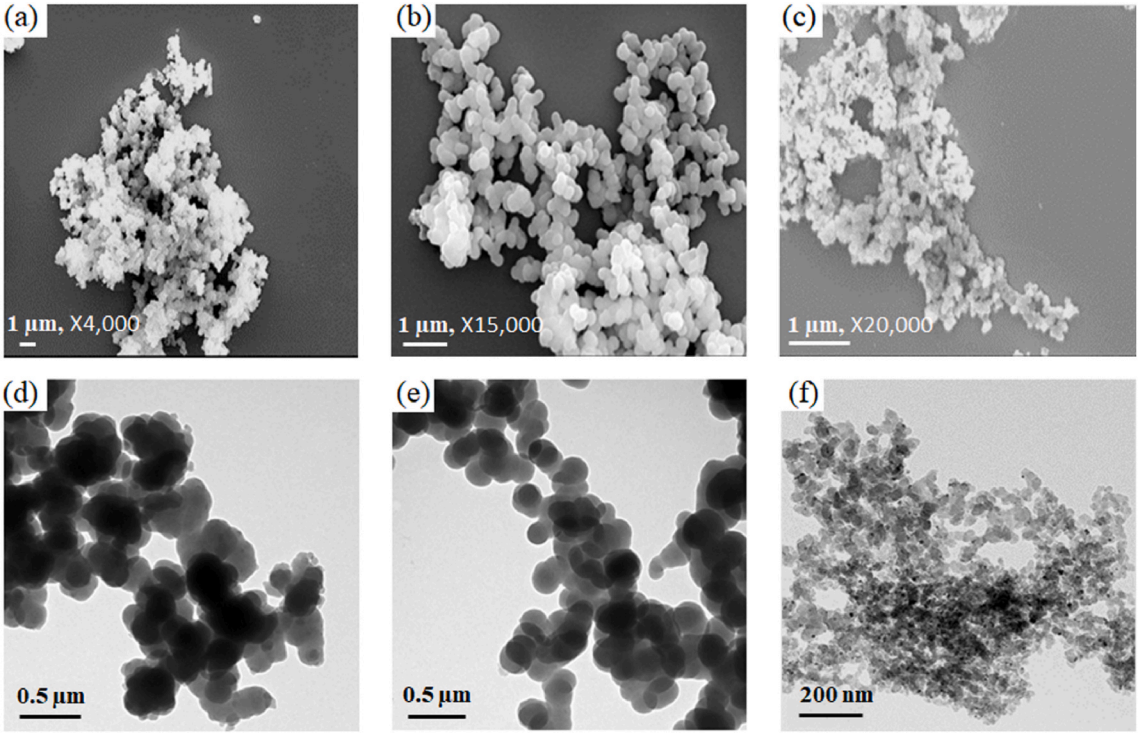

Fig. 3. SEM photos of (a) Cz-Cz, (b) Cz-TPA, and (c) Cz-TP CMPs; TEM photos of (d) Cz-Cz, (e) Cz-TPA, and (f) Cz-TP CMPs.

have nearly the same chemical composition, similar surface areas, and identical nitrogen content, but different specific capacitance were noticed. This was in fact as a result of different planarity between Cz-3Br, and TPA-3Br monomers and hence their corresponding polymers that resulted in different capacitance [58]. The resultant specific capacities were superior to those of other porous materials (Table S2). Fig. 5 explained the GCD profiles of the polymeric frameworks at diverse current density (0.5–20 A g^{-1}). Nearly triangular-shaped GCD curves were revealed for all synthesized CMPs, which confirms the suggestion of EDCL as the major mechanism for storing energy [Fig. 4(d-f)]. The Cz-TPA, and Cz-TP CMPs were proved to be the excellent choice for using as electrode material, owing to the longest discharge time than that of Cz-Cz CMP at all current densities. Furthermore, at 10 A g^{-1}, Cz-TPA CMP was found to have an effective average stability of 99.87%

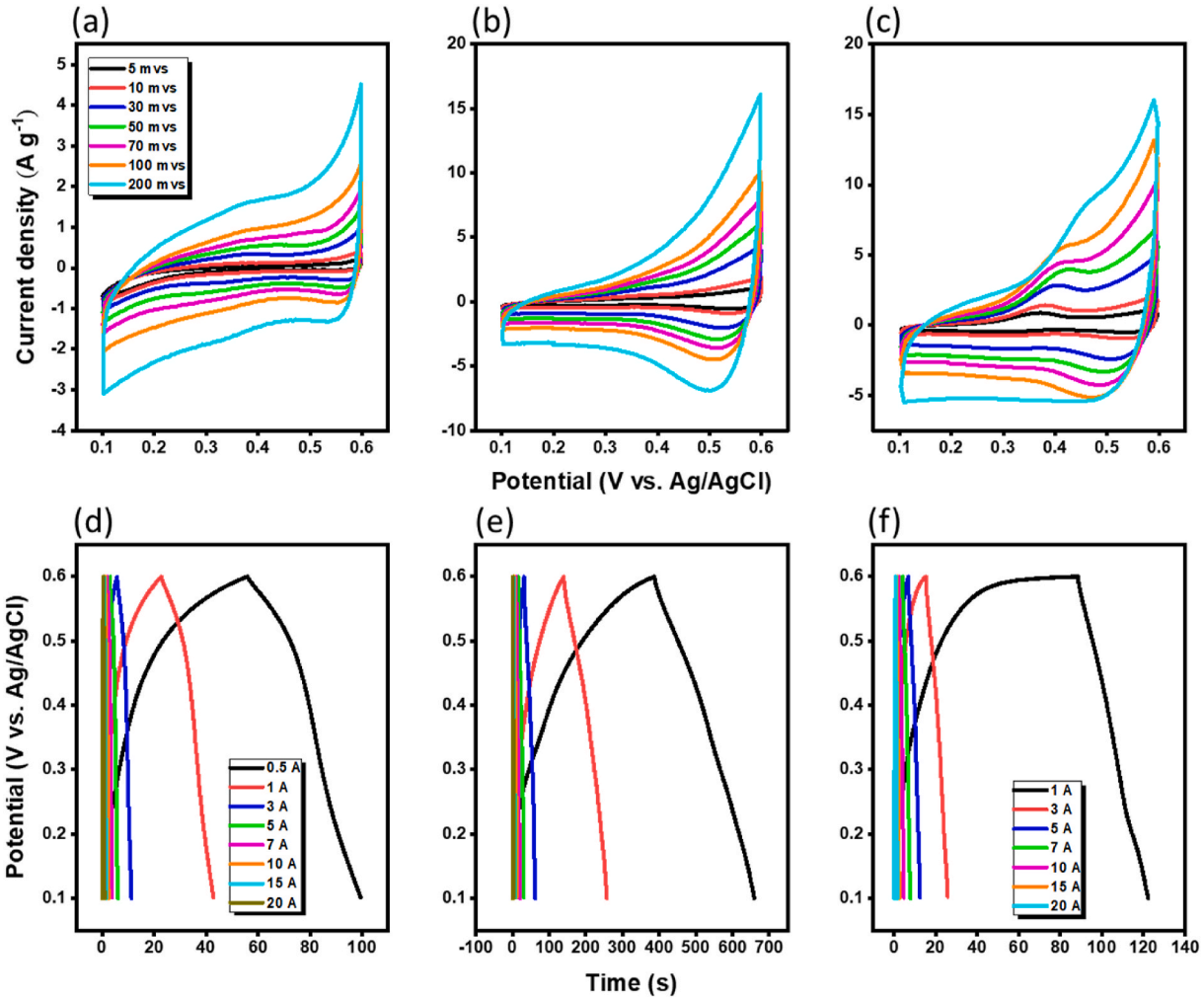

Fig. 4. CV curves of (a) Cz-Cz, (b) Cz-TPA, and (c) Cz-TP CMPs; The corresponding GCD profiles of (d) Cz-Cz, (e) Cz-TPA, and (f) Cz-TP CMPs, recorded at various currents.

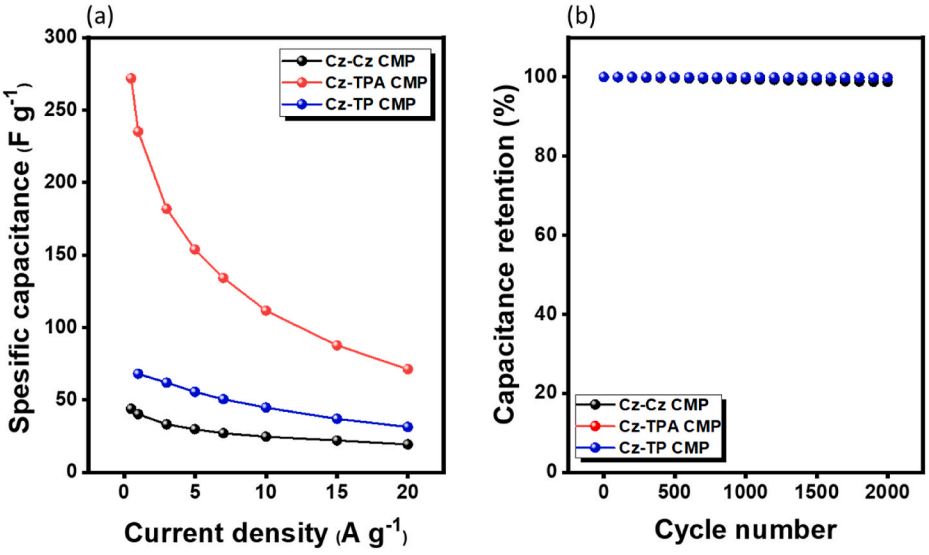

Fig. 5. (a) Specific capacitances of the carbazole-based CMPs recorded at current densities from 0.5 to 20 A g^{-1}. (b) Cycling stabilities of the CMPs electrodes, recorded at a current density of 10 A g^{-1} over 2000 cycles.

after 2000 cycles, while the Cz-Cz and Cz-TP CMPs represented slightly lower values of average stability to be 98.78%, and 99.86%, respectively, at the same conditions [Fig. 5(b)]. By matching these values with those of reported stable electrodes such as metal oxides [59,60] and MOF-derived metal oxides [61–63], the prepared conjugated polymers were among the best stable electrode materials.

4. Conclusion

A new series of electrochemically active polymers based on a nitrogen-rich carbazole moiety have been developed, built, and tested as effective electrodes for high-performance supercapacitors. The existing nitrogen atoms induced pseudocapacitance by promoting the charge mobility and insertion of negative charges on the surfaces of polymer frameworks. The obtained carbazole-based CMPs represented prime thermal stabilities and char yields, as well as outstanding surface areas according to TGA and BET measurements. Cz-TPA CMP have the highest specific capacitance of 271.82 F g^{-1} at 0.5 A g^{-1} current density with a capacitance retention of 99.87% over 2000 cycles at current density of 10 A g^{-1}. These findings of excellent capacitance and sturdy cycle life provide insights for the future design and synthesis of N-rich electroactive CMPs to be used in energy storage devices.

CRediT authorship contribution statement

Ahmed F. Saber: Investigation, Methodology, Writing – original draft. **Santosh U. Sharma:** Investigation, Methodology, Writing – original draft. **Jyh-Tsung Lee:** Investigation, Methodology, Conceptualization, Supervision, Writing – original draft. **Ahmed F.M. EL-Mahdy:** Conceptualization, Supervision, Writing – review & editing. **Shiao-Wei Kuo:** Conceptualization, Supervision, Writing – review & editing.

Declaration of competing interest

The authors declare that they have no known competing financial interests or personal relationships that could have appeared to influence the work reported in this paper.

Acknowledgments

This study was supported financially by the Ministry of Science and Technology, Taiwan, under contracts MOST 108-2638-E-002-003-MY2, and 108-2221-E-110-014-MY3. The authors thank the staff at National Sun Yat-sen University for their assistance with TEM (ID: EM022600) experiments.

Appendix A. Supplementary data

Supplementary data to this article can be found online at https://doi.org/10.1016/j.polymer.2022.125070.

References

[1] J. Skea, S. Nishioka, Policies and practices for a low-carbon society, Clim. Policy 8 (2008) 5–16.
[2] L. Li, F. Lu, R. Xue, B.L. Ma, Q. Li, N. Wu, H. Liu, W.Q. Yao, H. Guo, W. Yang, Ultrastable triazine-based covalent organic framework with an interlayer hydrogen bonding for supercapacitor applications, ACS Appl. Mater. Interfaces 11 (2019) 26355–26363.
[3] S. Najib, E. Erdem, Current progress achieved in novel materials for supercapacitor electrodes: mini review, Nanoscale Adv. 1 (2019) 2817–2827.
[4] F. Wang, X. Wu, X. Yuan, Z. Liu, Y. Zhang, L. Fu, Y. Zhu, Q. Zhou, Y. Wu, W. Huang, Latest advances in supercapacitors: from new electrode materials to novel device designs, Chem. Soc. Rev. 46 (2017) 6816–6854.
[5] X.Y. Tao, J. Du, Y. Sun, S.L. Zhou, Y. Xia, H. Huang, Y.P. Gan, W.K. Zhang, X.D. Li, Exploring the energy storage mechanism of high performance MnO_2 electrochemical capacitor electrodes: an in situ atomic force microscopy study in aqueous electrolyte, Adv. Funct. Mater. 37 (2013) 4745–4751.
[6] P. Simon, Y. Gogotsi, Capacitive energy storage in nanostructured carbon-electrolyte systems, Acc. Chem. Res. 46 (2013) 1094–1103.
[7] A.M. Khattak, H. Sin, Z.A. Ghazi, X. He, B. Liang, N.A. Khan, H.R. Alanagh, A. Iqbal, L.S. Li, Z.T. Tang, Controllable fabrication of redox-active conjugated microporous polymer on reduced graphene oxide for high performance faradaic energy storage, J. Mater. Chem. 6 (2018) 18827–18832.
[8] F. Béguin, V. Presser, A. Balducci, E. Frackowiak, Carbons and electrolytes for advanced supercapacitors, Adv. Mater. 26 (2014) 2219–2251.
[9] P. Simon, Y. Gogotsi, B. Dunn, Where do batteries end and supercapacitors begin? Science 343 (2014) 1210–1211.
[10] J. Yan, Q. Wang, T. Wei, Z.J. Fan, Recent advances in design and fabrication of electrochemical supercapacitors with high energy densities, Adv. Energy Mater. 4 (2014) 1300816–1300859.
[11] N. Manjunatha, M. Imadadulla, K.S. Lokesh, K.R. Reddy, Synthesis and electropolymerization of tetra-[β-(2-benzimidazole)] and tetra-[β-(2-(1-(4-aminophenyl))benzimidazole)] embedded cobalt phthalocyanine and their supercapacitance behaviour, Dyes Pigments 153 (2018) 213–224.
[12] Y.G. Wang, Y.F. Song, Y.Y. Xia, Electrochemical capacitors: mechanism, materials, systems, characterization and applications, Chem. Soc. Rev. 45 (2016) 5925–5950.
[13] C. Acar, I. Dincer, Comparative assessment of hydrogen production methods from renewable and non-renewable sources, Int. J. Hydrogen Energy 39 (2014) 1–12.
[14] C.D. Lokhande, D.P. Dubal, O.S. Joo, Metal oxide thin film based supercapacitors, Curr. Appl. Phys. 11 (2011) 255–270.
[15] W. Li, J. Liu, D. Zhao, Mesoporous materials for energy conversion and storage devices, Nat. Rev. Mater. 1 (2016) 16023–16040.
[16] Y. Li, S. Zheng, X. Liu, P. Li, L. Sun, R. Yang, S. Wang, Z. Wu, X. Bao, W.Q. Deng, Conductive microporous covalent triazine-based framework for high-performance electrochemical capacitive energy storage, Angew. Chem. Int. Ed. 57 (2018) 7992–7996.
[17] R.Y. Shi, C.P. Han, H. Duan, L. Xu, D. Zhou, H.F. Li, J.Q. Li, F.Y. Kang, B.H. Li, G. X. Wang, Redox-active organic sodium anthraquinone-2-sulfonate (AQS) anchored on reduced graphene oxide for high-performance supercapacitors, Adv. Energy Mater. 31 (2018) 1802088–1802097.
[18] H.R. Abuzeid, A.F.M. EL-Mahdy, S.-W. Kuo, Covalent organic frameworks: design principles, synthetic strategies, and diverse applications, Giant 6 (2021), 100054.
[19] A.F.M. EL-Mahdy, C. Young, J. Kim, J. You, Y. Yamauchi, S.-W. Kuo, Hollow microspherical and microtubular [3+3] carbazole-based covalent organic frameworks and their gas and energy storage applications, ACS Appl. Mater. Interfaces 11 (2019) 9343–9354.
[20] M.G. Mohamed, A.F.M. EL-Mahdy, M.G. Kotp, S.-W. Kuo, Advances in porous organic polymers: syntheses, structures, and diverse applications, Mater. Adv. 3 (2022) 707–733.
[21] M.M. Samy, M.G. Mohamed, T.H. Mansoure, T.S. Meng, M.A.R. Khan, C.C. Liaw, S.-W. Kuo, Solid state chemical transformations through ring-opening polymerization of ferrocene-based conjugated microporous polymers in host–guest complexes with benzoxazine-linked cyclodextrin, J. Taiwan Inst. Chem. Eng. 132 (2022), 104110.
[22] M.G. Mohamed, M.M. Samy, T.H. Mansoure, S.U. Sharma, M.S. Tsai, J.H. Chen, J. T. Lee, H.-H. Yu, T. Chen, S.-W. Kuo, Dispersions of 1, 3, 4-oxadiazole-linked conjugated microporous polymers with carbon nanotubes as a high-performance electrode for supercapacitors, ACS Appl. Energy Mater. 5 (2022) 3677–3688.
[23] M.G. Mohamed, S.U. Sharma, N.Y. Liu, T.H. Mansoure, M.M. Samy, S.V. Chaganti, Y.L. Chang, J.T. Lee, S.-W. Kuo, Ultrastable covalent triazine organic framework based on anthracene moiety as platform for high-performance carbon dioxide adsorption and supercapacitors, Int. J. Mol. Sci. 23 (2022) 3174.
[24] M.G. Mohamed, A.F.M. EL-Mahdy, Y. Takashi, S.-W. Kuo, Ultrastable conductive microporous covalent triazine frameworks based on pyrene moieties provide high-performance CO_2 uptake and supercapacitance, New J. Chem. 44 (2020) 8241–8253.
[25] M.G. Mohamed, X. Zhang, T.H. Mansoure, A.F.M. EL-Mahdy, C.-F. Huang, M. Danko, Z. Xin, S.-W. Kuo, Hypercrosslinked porous organic polymers based on tetraphenylanthraquinone for CO_2 uptake and high-performance supercapacitor, Polymer 205 (2020) 122857–122868.
[26] A.F.M. EL-Mahdy, M.B. Zakaria, H.-X. Wang, T. Chen, Y. Yamauchi, S.-W. Kuo, Heteroporous bifluorenylidene-based covalent organic frameworks displaying exceptional dye adsorption behavior and high energy storage, J. Mater. Chem. 8 (2020) 25148–25155.
[27] Y.-G. Wang, H.-Q. Li, Y.-Y. Xia, Ordered whiskerlike polyaniline grown on the surface of mesoporous carbon and its electrochemical capacitance performance, Adv. Mater. 18 (2006) 2619–2623.
[28] L.L. Zhang, X.S. Zhao, Carbon-based materials as supercapacitor electrodes, Chem. Soc. Rev. 38 (2009) 2520–2531.
[29] I.-H. Kim, J.-H. Kim, Y.-H. Lee, K.-B. Kim, Synthesis and characterization of electrochemically prepared ruthenium oxide on carbon nanotube film substrate for supercapacitor applications, J. Electrochem. Soc. 152 (2005) A2170.
[30] Y. Zhou, Z.-Y. Qin, L. Li, Y. Zhang, Y.-L. Wei, L.-F. Wang, M.-F. Zhu, Polyaniline/multi-walled carbon nanotube composites with core–shell structures as supercapacitor electrode materials, Electrochim. Acta 55 (2010) 3904–3908.
[31] M. Khalid, H. Varela, A general potentiodynamic approach for red phosphorus and sulfur nanodot incorporation on reduced graphene oxide sheets: metal-free and binder-free electrodes for supercapacitor and hydrogen evolution activities, J. Mater. Chem. 6 (2018) 3141–3150.
[32] J.Y. Cao, Y. Zhao, Y.F. Xu, Y. Zhang, B. Zhang, H.S. Peng, Sticky-note supercapacitors, J. Mater. Chem. 6 (2018) 3355–3360.
[33] A.G. Tabrizi, N. Arsalani, A. Mohammadi, H. Namazi, L.S. Ghadimi, I. Ahadzadeh, Facile synthesis of a $MnFe_2O_4$/rGO nanocomposite for an ultra-stable symmetric supercapacitor, New J. Chem. 41 (2017) 4974–4984.

[34] H. Ahn, Y.C. Huang, C.W. Lin, Y.H. Lee, Efficient defect healing of transition metal dichalcogenides by metallophthalocyanine, ACS Appl. Mater. Interfaces 10 (2018) 29145–29152.
[35] A.M. Khattak, H. Sin, Z.A. Ghazi, X. He, B. Liang, N.A. Khan, H.R. Alanagh, A. Iqbal, L. Li, Z. Tang, Controllable fabrication of redox-active conjugated microporous polymer on reduced graphene oxide for high performance faradaic energy storage, J. Mater. Chem. 6 (2018) 18827–18832.
[36] A.F. Saber, A.F.M. EL-Mahdy, (E)-1, 2-Diphenylethene-based conjugated nanoporous polymers for a superior adsorptive removal of dyes from water, New J. Chem. 45 (2021) 21834–21843.
[37] B. Zhou, F. Yan, X. Li, J. Zhou, W. Zhang, An interpenetrating porous organic polymer as a precursor for FeP/Fe_2P-embedded porous carbon toward a pH-universal ORR catalyst, ChemSusChem 12 (2019) 915–923.
[38] Y. Xu, N. Mao, C. Zhang, X. Wang, J.H. Zeng, Y. Chen, F. Wang, J.X. Jiang, Rational design of donor-π-acceptor conjugated microporous polymers for photocatalytic hydrogen production, Appl. Catal. B Environ. 228 (2018) 1–9.
[39] T.L. Lee, A.M. Elewa, M.G. Kotp, H.H. Chou, A.F.M. El-Mahdy, Carbazole-and thiophene-containing conjugated microporous polymers with different planarity for enhanced photocatalytic hydrogen evolution, Chem. Commun. 57 (2021) 11968–11971.
[40] A.M. Elewa, A.F.M. EL-Mahdy, M.H. El-sayed, M.G. Mohamed, S.-W. Kuo, H.-H. Chou, Sulfur-doped triazine-conjugated microporous polymers for achieving the robust visible-light-driven hydrogen evolution, Chem. Eng. J. 421 (2021) 129825–129837.
[41] A.M. Elewa, M.H. El-sayed, A.F.M. EL-Mahdy, C.-L. Chang, L.-Y. Ting, W.-C. Lin, C.-Y. Lu, H.-H. Chou, Triptycene-based discontinuously-conjugated covalent organic polymer photocatalysts for visible-light-driven hydrogen evolution from water, Appl. Catal., B 285 (2021) 119802–119814.
[42] M.G. Kotp, A.M. Elewa, A.F.M. EL-Mahdy, H.H. Chou, S.W. Kuo, Tunable pyridyl-based conjugated microporous polymers for visible light-driven hydrogen evolution, ACS Appl. Energy Mater. 4 (2021) 13140–13151.
[43] A.F. Saber, K.-Y. Chen, A.F.M. EL-Mahdy, S.-W. Kuo, Designed azo-linked conjugated microporous polymers for CO_2 uptake and removal applications, J. Polym. Res. 28 (2021) 1–12.
[44] M.M. Samy, M.G. Mohamed, A.F.M. El-Mahdy, T.H. Mansoure, K.C.-W. Wu, S.-W. Kuo, High-performance supercapacitor electrodes prepared from dispersions of tetrabenzonaphthalene-based conjugated microporous polymers and carbon nanotubes, ACS Appl. Mater. Interfaces 13 (2021) 51906–51916.
[45] N. Chaoui, M. Trunk, R. Dawson, J. Schmidt, A. Thomas, Trends and challenges for microporous polymers, Chem. Soc. Rev. 46 (2017) 3302–3321.
[46] A.M. Khattak, H. Sin, Z.A. Ghazi, X. He, B. Liang, N.A. Khan, H.R. Alanagh, A. Iqbal, L.S. Li, Z.Y. Tang, Controllable fabrication of redox-active conjugated microporous polymers on reduced graphene oxide for high performance faradaic energy storage, J. Mater. Chem. 6 (2018) 18827–18832.
[47] A.F.M. EL-Mahdy, T.C. Yu, S.W. Kuo, Synthesis of multiple heteroatom–doped mesoporous carbon/silica composites for supercapacitors, Chem. Eng. J. 414 (2021) 128796–128811.
[48] A.F.M. EL-Mahdy, T.C. Yu, M.G. Mohamed, S.W. Kuo, Secondary structures of polypeptide-based diblock copolymers influence the microphase separation of templates for the fabrication of microporous carbons, Macromolecules 54 (2021) 1030–1042.
[49] K. Yuan, X. Zhuang, H. Fu, G. Brunklaus, M. Forster, Y. Chen, X. Feng, U. Scherf, Two-dimensional core-shelled porous hybrids as highly efficient catalysts for the oxygen reduction reaction, Angew. Chem., Int. Ed. 55 (2016) 6858–6863.
[50] A.F.M. El-Mahdy, J. Lüder, M.G. Kotp, S.W. Kuo, A Tröger's base-derived covalent organic polymer containing carbazole units as a high-performance supercapacitor, Polymers 13 (2021) 1385–1398.
[51] J.P. Paraknowitsch, A. Thomas, Doping carbons beyond nitrogen: an overview of advanced heteroatom doped carbons with boron, sulphur and phosphorus for energy applications, Energy Environ. Sci. 6 (2013) 2839–2855.
[52] K.N. Wood, R. O'Hayre, S. Pylypenko, Recent progress on nitrogen/carbon structures designed for use in energy and sustainability applications, Energy Environ. Sci. 7 (2014) 1212–1249.
[53] M.R. Talipov, M.M. Hossain, A. Boddeda, K. Thakura, R. Rathore, A search for blues brothers: X-ray crystallographic/spectroscopic characterization of the tetraarylbenzidine cation radical as a product of aging of solid magic blue, Org. Biomol. Chem. 14 (2016) 2961–2968.
[54] M.G. Mohamed, M.H. Elsayed, A.M. Elewa, A.F.M. EL-Mahdy, C.-H. Yang, A.A. K. Mohammed, H.-H. Chou, S.-W. Kuo, Pyrene-containing conjugated organic microporous polymers for photocatalytic hydrogen evolution from water, Catal. Sci. Technol. 11 (2021) 2229–2241.
[55] N.I. Abdo, A.A. El-Shehawy, A.A. El-Barbary, J.-S. Lee, Palladium-catalyzed direct C–H arylation of thieno[3,4-*b*]pyrazines: synthesis of advanced oligomeric and polymeric materials, Eur. J. Org. Chem. 2012 (2012) 5540–5551.
[56] R. Heimböckel, F. Hoffmann, M. Fröba, Insights into the influence of the pore size and surface area of activated carbons on the energy storage of electric double layer capacitors with a new potentially universally applicable capacitor model, Phys. Chem. Chem. Phys. 21 (2019) 3122–3133.
[57] R. Kötz, M. Carlen, Principles and applications of electrochemical capacitors, Electrochim. Acta 45 (2000) 2483–2498.
[58] W. Yang, B. Huang, L. Li, K. Zhang, Y. Li, J. Huang, X. Tang, T. Hu, K. Yuan, Y. Chen, Covalently sandwiching MXene by conjugated microporous polymers with excellent stability for supercapacitors, Small Methods (2020), 2000434.
[59] X. Xia, S. Deng, D. Xie, Y. Wang, S. Feng, J. Wu, J. Tu, Boosting sodium ion storage by anchoring MoO_2 on vertical graphene arrays, J. Mater. Chem. 6 (2018) 15546–15552.
[60] X. Xia, S. Deng, S. Feng, J. Wu, J. Tu, Hierarchical porous $Ti_2Nb_{10}O_{29}$ nanospheres as superior anode materials for lithium ion storage, J. Mater. Chem. 5 (2017) 21134–21139.
[61] R.R. Salunkhe, Y.V. Kaneti, Y. Yamauchi, Metal–organic framework-derived nanoporous metal oxides toward supercapacitor applications: progress and prospects, ACS Nano 11 (2017) 5293–5308.
[62] R.R. Salunkhe, J. Tang, N. Kobayashi, J. Kim, Y. Ide, S. Tominaka, J.H. Kim, Y. Yamauchi, Ultrahigh performance supercapacitors utilizing core–shell nanoarchitectures from a metal–organic framework-derived nanoporous carbon and a conducting polymer, Chem. Sci. 7 (2016) 5704–5713.
[63] C. Young, J. Wang, J. Kim, Y. Sugahara, J. Henzie, Y. Yamauchi, Controlled chemical vapor deposition for synthesis of nanowire arrays of metal–organic frameworks and their thermal conversion to carbon/metal oxide hybrid materials, Chem. Mater. 30 (2018) 3379–3386.